Supplementary material

We present next the full methodology used to prepare the systems used in this study and and additional figures.

SI. FULL SIMULATION METHODOLOGY

SI. 1. Preparation of amorphous silica surfaces

The amorphous silica surfaces are generated first with a combination of MD methods and then with DFT geometry optimisations. The MD procedure is composed of two steps. In the first step, we generate an amorphous cube using a typical melting and quenching technique with the classical molecular package LAMMPS. [1] The interatomic forces are calculated with the potential for SiO_2 parameterised by Nakano et al.[2], which has been shown to provide an accurate description of the amorphous phase at a low computational cost. We initially replicate the unit cell 3x3x2 times in the beta-cristobalite lattice. The temperature of the resulting parallelepiped is then heat up from 300 K to 5100 K using a constant volume and temperature scheme. Each time step is 0.25×10^{-3} ps and periodic boundary conditions are applied in the x, y, and z directions. Once the parallelepiped is at 5100 K, we modify its cross section which now has a side length of 1.623 nm and then quench it to 300 K in three stages, where in each one the temperature is cooled down 700 K at constant pressure and temperature in 2×10^5 steps and then letting the system relax at constant volume and energy for another 2×10^5 steps. The fully-periodic amorphous cube has a density of 2.18 g/cm^3, which is in excellent agreement with the experimental value of 2.20 g/cm^3.

In the second step, we prepare slabs of amorphous silica in a two-stage process. In the first stage, we use the classical molecular package LAMMPS [3] to generate a bulk system made with 3x3x2 unit cells in the beta-cristobalite lattice. We then follow a melting-quench process to yield an amorphous cube has a density of 2.18 g/cm^3, close to the experimental value of 2.20 g/cm^3. The resulting configuration is then imported to the Materials Studio package[4], where a vacuum gap of 2 nm is imposed in the z-direction to create two surfaces. We then bridge a small number of Si atoms to four O atoms on the surface and in the inner regions of the slab. We next optimise the geometry with the COMPASS2[5] force field available in the Forcite Module and then with the DFTB+ Module and finally with ab-initio package CP2k[6] in its QUICKSTEP[7] implementation. CP2k uses the exchange-correlation functional in the generalised gradient approximation (GGA) formulated by Perdew et al. revised for solids and surfaces[8] (PBEsol), GTH pseudopotentials[9,10], and double-ζ basis sets with polarization functions (DZVP).[11] We used a threshold of 1×10^{-5} Ha, a cut-off of 500 Ry for the plane wave basis set, and a Grimme scheme[12] to include long-range forces. The optimisation is completed when the variation of the maximum force component of the current configuration is less than 1 x 10^{-3} Ha/Bohr. This bridging and optimisation is repeated until the surface is stable at which point we run an ab-initio molecular dynamics simulation with CP2k with a timestep of 0.25×10^{-3} ps. The final Q^4 (no dangling silanol Si-OH groups) surface has a

cross section of 1.578 nm x 1.572 nm in the y and z directions and a length of 2.475 nm in the x-direction. We believe that this length is sufficiently long to reproduce bulk-like conditions in the inner layers of this silica slab as Goumans et al.[13] showed that a slab of quartz-silica with a thickness of 1.125 nm is sufficiently large to represent bulk-like behaviour in the innermost layers. The average bond length between Si and O atoms is 0.163 nm and the average angle between a silicon and two neighbouring oxygens is 109.43 degrees.[14]

We use this Q^4 surface to create others with Q^3/Q^4 chemistries, in which a few Si-O are broken in the Q^4 surface and replaced with silanol Si-OH groups with concentrations of up to 6.86 groups per nm^2.[15] Once the silanol groups are built, the slabs are optimised with CP2k and run with ab initio molecular dynamics again.

SI. 2. Preparation of amorphous polyethylene surfaces

The amorphous polyethylene systems are also prepared using the Materials Studio software using four chains of 40 carbons with the COMPASS2 force field. The amorphous solid has the same cross section as the amorphous silica slab and a depth of 1.76 nm. Chains are not allowed to cross the boundaries in the x direction to avoid splitting the chains when a vacuum gap of 2.0 nm is imposed (see later) though periodic boundary conditions are still applied in all three directions. These configurations are then relaxed with CP2k with the local-density approximation (LDA) and the long-range forces are described by the Dion-Rydberg-Schroeder-Langreth-Lundqvist (DRSLL) nonlocal van der Waals density functional. [16] After the structure is optimised, we run a short ab initio molecular dynamics simulation of 1 ps to further relax the structure.

SI. 3. Preparation of water systems

Ensembles of liquid water at 300 K are first prepared using the TIP04/2005 model,[17] which gives excellent density predictions at 278 K. The system is composed of 150 molecules, occupying a parallelepiped region with the same cross section as the silica and polyethylene samples. We next run an ab-initio molecular dynamics simulation with CP2k for 25 ps with a timestep of 0.25×10^{-3} ps to relax the bond lengths with the PBE[18] functional revised for small molecules (revPBE[19]) in the bulk and, with a vacuum gap of 2.0 nm, to create a water/vapour interface. We have used the revPBE functional because from side tests with a cubic system of 343 molecules at constant temperature 300 K and pressure of 1 bar, we have found that this revised form improves significantly the agreement with the experimental density with respect to the original parameterisation PBE: the disagreement is only 3.90 % using revPBE, whereas it deviates up to 13.39% with PBE. Note though that the high computational cost of these ab-initio molecular dynamics calculations restricts the length of time for which we can simulate these water systems. 1 ps of simulated time with CP2k needs to be run on 64 processors for nearly 10 hours for the bulk phase and 13 hours with the 2.0-nm vacuum gap.

SI. 4. Preparation of interfacial systems

Once the pure systems are obtained, we build interfaces of water/polyethylene, silica/polyethylene, and silica/water/silica interfaces. The first type is prepared with no vacuum using the revPBE functional and Grimme scheme. The second is prepared with and without a 2.0-nm vacuum gap, which requires to use the LDA/DRSLL setup for the former and the PBEsol[20]/Grimme for the latter. The use of LDA is justified because the polymer chains evaporates over a few ps of simulation. The third type of interfaces is prepared with the same vacuum gap and employs the revPBE functional. Once the computational setup is ready, the geometry of each two-component system is optimised with CP2k to avoid undesirable orbital overlapping between the atoms at each surface. Thanks to this optimisation, the systems require a shorter simulation time to equilibrate. The systems are run in C2PK for 7.5 ps for polyethylene/silica and 15 ps for polyethylene/water and water/silica/water to obtain a sufficient number of configurations with a timestep of 0.25×10^{-3} ps.

The resulting configurations from the ab-initio molecular dynamics run are then used by the CRYSTAL17 DFT code[21]. The DFT calculations are carried out using the hybrid B3LYP exchange-correction functional. A standard all-electron 6-31G**[22,23] basis set is used to represent the local atomic orbitals in terms of primitive Cartesian Gaussian functions. Polarization functions (p-functions for hydrogens and d-functions for carbons, oxygens, and silicons) are used to ensure that the orbitals can distort from their original atomic symmetry, and to adapt to the molecular surroundings leading to a better prediction of the total energy of the system with high hydrogen content. [24] Reciprocal space integrations are restricted to the Γ-point of the Brillouin zone and a ground-state energy convergence is enforced at 1×10^{-6} Ha. Standard parameters for two-electron integral calculations are used throughout.

Periodic boundary conditions are imposed on the x, y, z directions in systems with no vacuum using the keyword CRYSTAL and on the x and y directions in systems with a 2.0-nm vacuum gap using the keyword SLAB. We refer hereinafter as '3D-periodic' to the first type of simulations and '2D-slab' to the second. We use this second type of calculations in systems where surface dipoles are present, such as liquid water or silica slabs with hydroxylated walls, to obtain a well-defined vacuum level, where the zero of the electrostatic potential V_z is defined by the CRYSTAL code in such a way that $V_z(+\infty) = -V_z(-\infty)$. See, for example, the example with a slab of amorphous silica with a silanol surface concentration of 1.61 nm^{-2} in Fig. S1 in the supplementary material. In this case, the permanent dipole in the silica slab divides the space in two parts, with higher and lower potential, having two equally valid vacuum states. An electron extracted from the material will chose the side with a positive potential to have a negative (minimum) potential energy in the vacuum. Hence, we correct the energies of the LUMO using

$$LUMO_{\text{corrected}} = LUMO_{\text{uncorrected}} - e\langle V_z \rangle_{\text{vacuum}}, \quad (1)$$

where $LUMO_{corrected}$ and $LUMO_{uncorrected}$ are the correspondent corrected and uncorrected energies of this orbital, e the electron's charge, and $\langle V_z \rangle_{vacuum}$ is the positive average of the electrostatic potential. In addition, for systems with no dipoles, such as slabs of amorphous polyethylene or silica with no silanols, the LUMO energies are corrected with the following expression:

$$LUMO_{corrected} = LUMO_{uncorrected} - (E_{band\ 1,\ bulk\text{-}like} - E_{band\ 1,bulk}) - e\langle V_z \rangle_{vacuum}, \quad (2)$$

where the difference between $E_{band\ 1,bulk\text{-}like}$ and $E_{band\ 1,bulk}$ corresponds the core-level shift of the energies of the band 1 in the bulk case and the bulk-like region from a second simulation with a 2.0-nm vacuum gap with a Q^4 surface. Equation (2) is also applied to obtain excess electron energies for amorphous polyethylene slabs.

SI. 5. Calculation of Valence Band offsets

We use the Shi and Ramprasad's method to calculate Valence Band offsets (VBOs) as explained in Sec. III.3. We plot the HOMOs of each layer vs. its position perpendicular to the interface (e.g. z) and the valence band offset is taken as the maximum difference between the HOMOs in water and polyethylene (see Fig. S4):

$$VBO = \max(E_{HOMO,a\text{-}PE} - E_{HOMO,water}), \quad (3)$$

where $E_{HOMO,a\text{-}PE}$ is the energy of the HOMO in a slice of the amorphous polyethylene slab and $E_{HOMO,water}$ is the energy of the HOMO in a division of the water ensemble.

SI. 6. Calculation of Diffusion coefficients of one excess electron in liquid water

The calculation of the diffusion coefficients starts first by calculating the centre of mass of the LUMO in each of the 61 configurations collected between 10 and 25 ps in intervals of 0.25 ps. Once all centres of mass $r_{CM}(t) = \{x_{CM}(t), y_{CM}(t), z_{CM}(t)\}$ are calculated for each time t, we then compute the mean square displacement MSD(t) from the initial time t_0 using the expression

$$MSD(t) = [x_{CM}(t) - x_{CM}(t_0)]^2 + [y_{CM}(t) - y_{CM}(t_0)]^2 + [z_{CM}(t) - z_{CM}(t_0)]^2.$$

We then use the Einstein's formula:

$$D(t) = \lim_{t\to\infty} MSD(t)/6N_m t,$$

where N_m is the number of particles, which is equal to 1 as we have one electron, to calculate the diffusion coefficient $D(t)$ for each time as

$$D(t) = MSD(t)/6t.$$

We then average the values of MSD(t) and $D(t)$ over five different configurations of water to reduce the noise of their signals. The averaged MSD(t) and $D(t)$ are finally plotted as a function of time in Fig.s S2 and S3. Given that the signal of MSD(t) is very noisy to fit it with a line equation, we decided instead to fit the values of $D(t)$ between 15 and 25 ps, which show a well-defined flat value, to find the diffusion coefficient of the excess electron.

SUPPLEMENTARY FIGURES

Figure S1 (one column)

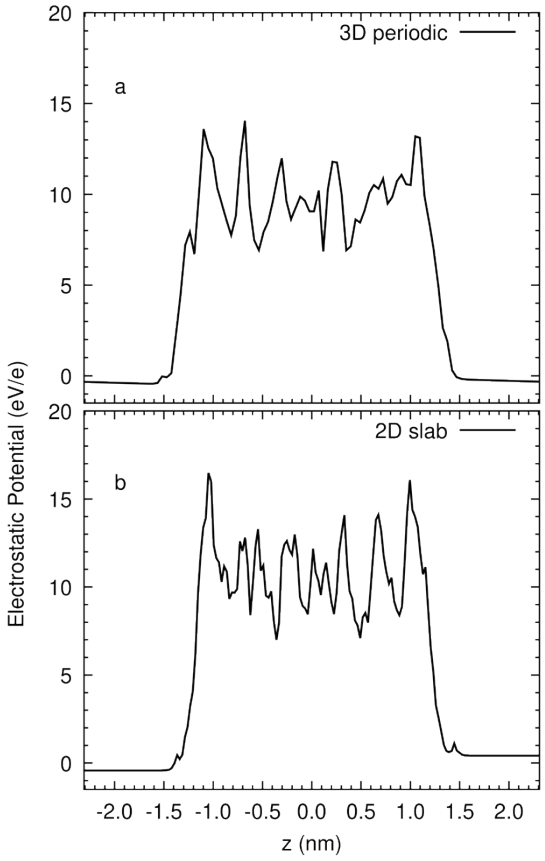

Figure S1. Average electrostatic potentials of an amorphous silica with 2.0 nm of vacuum whose surfaces Q^3/Q^4 has a silanol concentration of 1.61nm^{-2} calculated for with 3D-periodic (a) and 2D-slab CRYSTAL17 (b) calculations.

Figure S2 (one column)

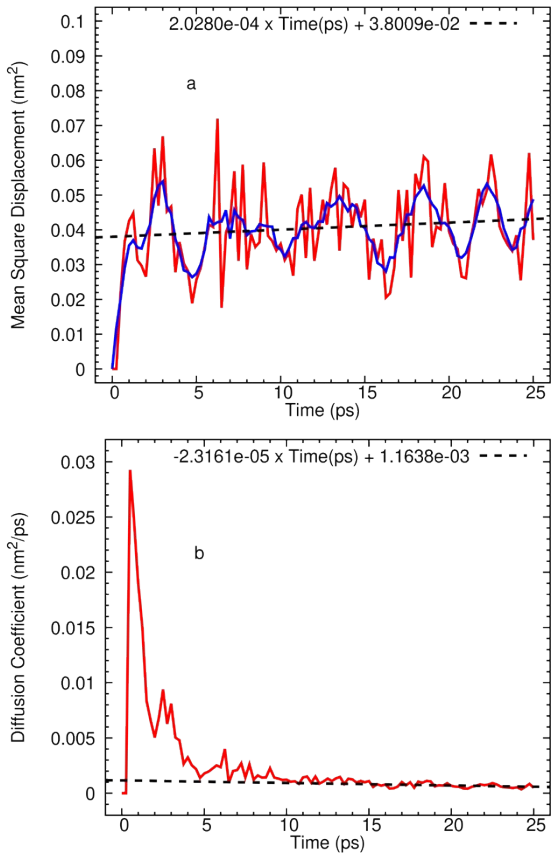

Figure S2. Mean square displacement (a) and diffusion coefficient (b) as a function of time obtained from five bulk configurations of 150 water molecules. Moving average of the mean square displacement is painted in blue and linear fitting to the non-averaged data is painted with a black dashed line.

Figure S3 (one column)

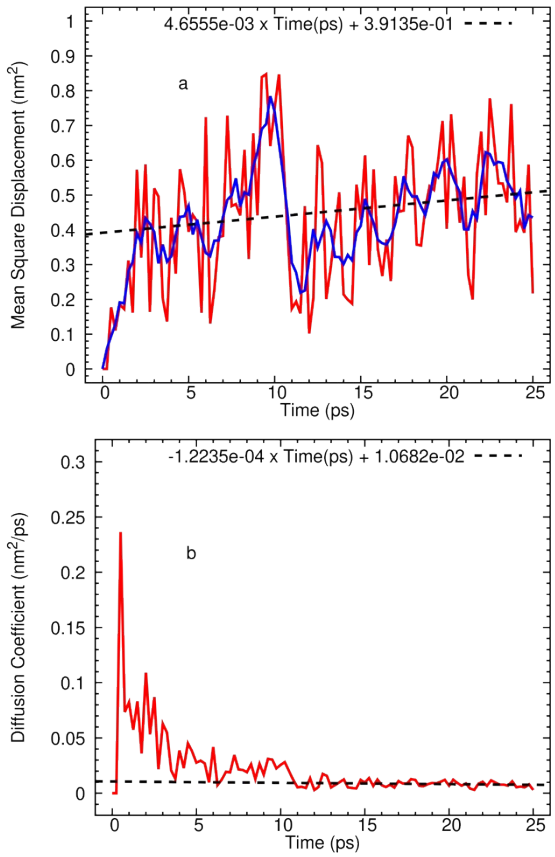

Figure S3. Mean square displacement (a) and diffusion coefficient (b) as a function of time obtained from one configuration of 150 water molecules with 2.0-nm vacuum. Moving average of the mean square displacement is painted in blue and linear fitting to the non-averaged data is painted with a black dashed line.

Figure S4 (one column)

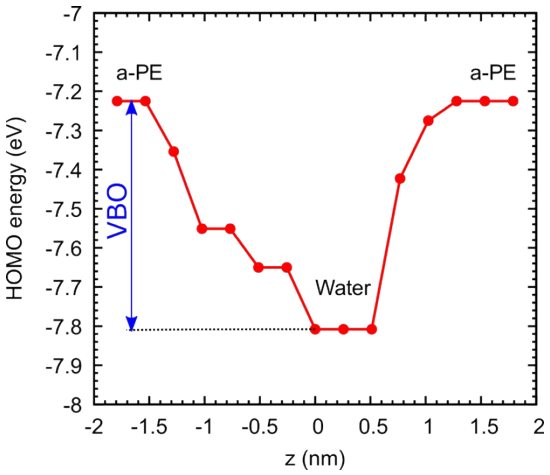

Figure S4. HOMO vs. z-direction in an interfacial water and polyethylene with no vacuum.

Figure S5 (one column)

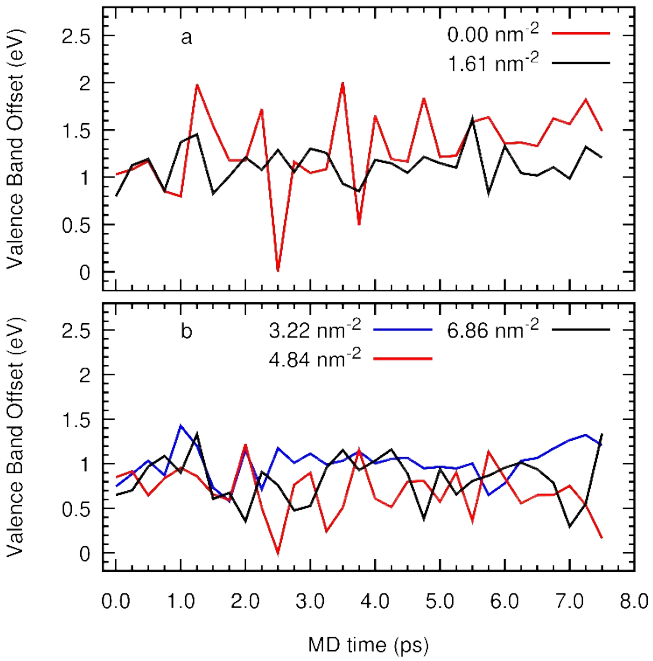

Figure S5. Valence band offset of an interfacial system of amorphous polyethylene and silica from a 3D-periodic calculation vs. time for silanol concentrations of 0.0 and 1.61 nm^{-2} in panel (a) and 3.22, 4.84, and 6.86 nm^{-2} in panel (b).

Figure S6 (one column)

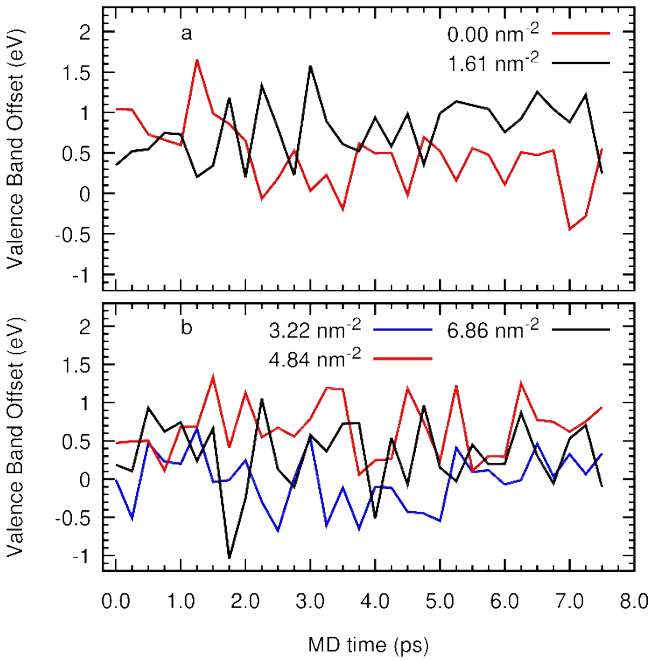

Figure S6. Valence band offset of an interfacial system of amorphous polyethylene and silica from a 2D-periodic calculation vs. time for silanol concentrations of 0.0 and 1.61 nm^{-2} in panel (a) and 3.22, 4.84, and 6.86 nm^{-2} in panel (b).

Figure S7 (one column)

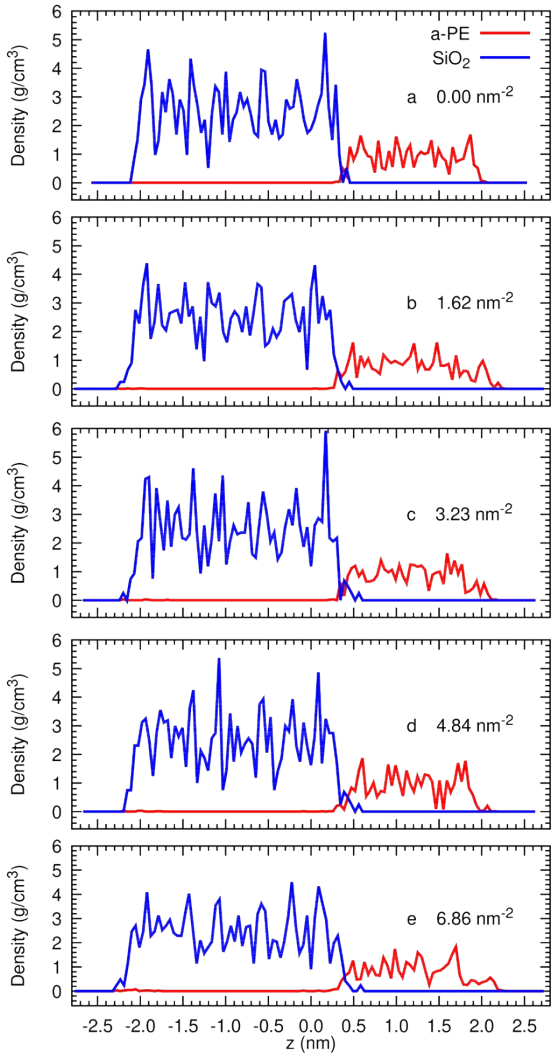

Figure S7. Average profile of the atomic density of the amorphous silica and polyethylene system at 7.5 ps of ab-initio molecular dynamics simulation.

Figure S8 (one column)

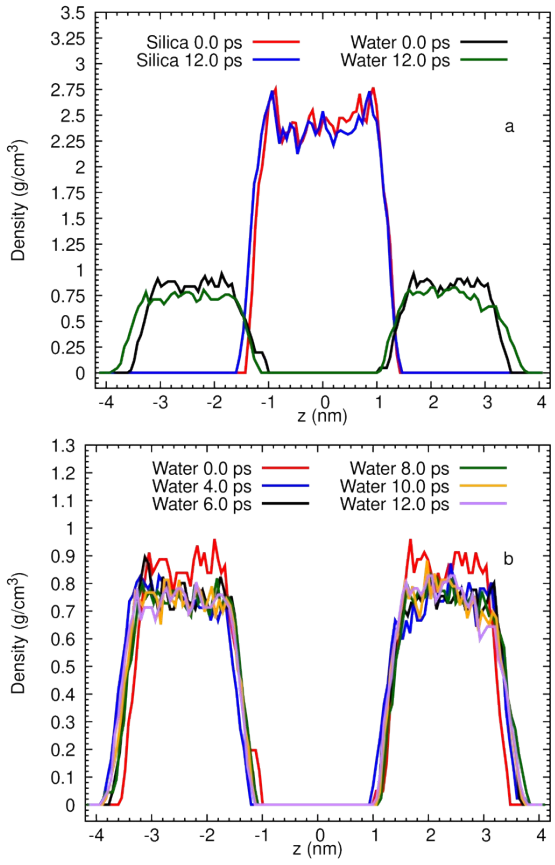

Figure S8. Average profile of the atomic density of the water/silica/water system along the z direction for different times from ab-initio molecular dynamics simulation.

REFERENCES

1 S. J. Plimpton, J. Comput. Phys. 117, 1 (1995).
2 A. Nakano, R. K. Kalia, and Vashishta, J. Non-Crystal. Solids 171, 157 (1994).
3 S. J. Plimpton, J. Comput. Phys., 1995, **117**, 1–19.
4 Dassault Systèmes BIOVIA, Materials Studio Suite, v.5.5.2, San Diego: Dassault Systèmes, 2017.
5 H. Sun, J. Phys. Chem. B, 1998, 102, 7338–7364.
6 J. Hutter, M. Iannuzzi, F. Schiffmann and J. VandeVondele, Comput. Mol. Sci., 2014, 4, 15–25.
7 J. VandeVondele, M. Krack, F. Mohamed, M. Parrinello, T. Chassaing and J. Hutter. Comp. Phys. Comm., 2005, 167, 103–128.
8 J. P. Perdew, A. Ruzsinszky, G. I. Csonka, O. A. Vydrov, G. E. Scuseria, L. A. Constantin, X. Zhou, and K. Burke, Phys. Rev. Lett. 100, 136406 (2008).
9 S. Goedecker, M. Teter, and J. Hutter, Phys. Rev. B 54, 1703 (1996).
10 M. Krack, Theor. Chem. Acc. 114, 145 (2005).
11 J. VandeVondele and J. Hutter, J. Chem. Phys. 127, 114105 (2007).
12 S. Grimme, J. Comp. Chem. 27, 1787 (2006).
13 T. P. M. Goumans, A. Wander, W. A. Brown and C. R. A. Catlow, Phys. Chem. Chem. Phys., 2007, 9, 2146–2152.
14 T. P. M. Goumans, A. Wander, W. A. Brown, C. R. A. Catlow, Phys. Chem. Chem. Phys. 9, 2146 (2007).
15 L. T. Zhuralev, Langmuir, 1987, 3, 316–318.
16 M. Dion, H. Rydberg, E. Schröder, D. C. Langreth and B. I. Lundqvist, Phys. Rev. Lett., 2005, 92, 246401.
17 J. L. Abascal and C. Vega, J. Chem. Phys., 2005, 123, 234505.
18 J. P. Perdew, K. Burke; M. Ernzerhof, Phys. Rev. Lett. 77 (1986), 3865–3868.
19 B. Hammer, L. B. Hansen and J. K. Nørskov, Phys. Rev. B, 1999, **59**, 7413.
20 J. P. Perdew, A. Ruzsinszky, G. I. Csonka, O. A. Vydrov, G. E. Scuseria, L. A Constantin, X. Zhou and K. Burke, Phys. Rev. Lett., 2008, **100**, 136406.
21 R. Dovesi, R. Orlando, A. Erba, C. M. Zicovich-Wilson, B. Civalleri, S. Casassa, L. Maschio, M. Ferrabone, M. De La Pierre, P. D'Arco, Y. Noel, M. Causa, M. Rerat and B. Kirtman, Int. J. Quantum Chem., 2014, **114**, 1287–1317.
22 G. A. Petersson, A. Bennett, T. G. Tensfeldt, M. A. Al-Laham, W . A. Shirley and J. Mantzaris, J. Chem. Phys., 1988, **89**, 2193–2218.
23 G. A. Petersson and M. A. Al-Laham, J. Chem. Phys., 1991, **94**, 6081–6090.
24 E. G. Lewards, Computational Chemistry, Springer, New York, 2nd edn, 2011, Ch. 5, pp. 232–255.